Evaluation of Mechanical and Durability Properties of RCC Containing Nano-Silica Through Non-Destructive Ultrasonic Pulse Velocity Method

¹Amirhesamaddin Armanpour, ²Mohammad Mahdi Amiri, ³Mohsen Adabi, ⁴Ehsan Darvishan

¹Department of Civil Engineering, Roudehen Branch, Islamic Azad University, Roudehen, Iran. Email: amirhesam.armanpour@gmail.com, https://orcid.org/0009-0006-6993-5375
 ²Department of Civil Engineering, Shahriar Branch, Islamic Azad University, Shahriar, Iran. Email: amiri@dena.kntu.ac.ir, https://orcid.org/0009-0006-6993-5375
 ³Department of Metallurgy and Materials Engineering, Roudehen, Islamic Azad University, Roudehen, Iran. Email: madabi@ut.ac.ir, https://orcid.org/0000-0001-7985-9114
 ⁴Department of Civil Engineering, Roudehen Branch, Islamic Azad University, Roudehen, Iran. Email: eh.darvishan@iau.ac.ir, https://orcid.org/0000-0003-2010-8919

Corresponding author: Mohammad Mahdi Amiri Email address: amiri@dena.kntu.ac.ir

Abstract

This research examined how the mechanical properties and longevity of roller compacted concrete are impacted by the particle size and dosage of nano-silica. The study involved substituting cement with NS at three different levels (1%, 3%, and 5%) using varying particle sizes of 8nm, 15nm, and 30nm. The study investigated the compressive and splitting tensile strengths of RCC incorporating NS after 7 and 28 days, as well as water absorption. Subsequently, freeze-thaw tests were conducted on RCC samples, with assessments of mass change, ultrasonic pulse velocity, and dynamic modulus of elasticity. Additionally, the microstructure of RCC specimens was analyzed through a scanning electron microscope. Findings revealed a decrease in compressive strength by 4.3% to 8.7% when increasing the particle size of 3% NS from 8nm to 15nm and 30nm. Moreover, an increase in NS dosage from 1% to 3% enhanced the splitting tensile strength of RCC from 2.88 MPa to 3.55 MPa for an 8nm NS particle size. Results indicated that incorporating up to 3% NS in RCC mixtures improved freeze-thaw resistance significantly. Analysis showed that NS dosage had a greater impact than particle size across all experiments. An artificial neural network model was developed to predict RCC's compressive strength under F-T cycles using parameters such as the number of F-T cycles, ultrasonic pulse velocity, and sample mass as inputs, demonstrating high predictive capability. Furthermore, Shapley additive explanations analysis was used to

assess the impact of input parameters on prediction accuracy, alongside discussions on sample imbalance's effect on prediction performance.

Keyword: Roller compacted concrete, Freeze-thaw resistance, Mechanical properties, Nano silica, Artificial neural network, SHAP analysis.

1. Introduction

The utilization of Roller Compacted Concrete (RCC), a type of dry concrete, is frequently chosen for construction of highway roads, airport runways, and dams because of its advantageous characteristics, which include low heat of hydration, cost-effectiveness, durability, and ease of application [1]. Although RCC is made of cement, water, fine and coarse aggregates, and similar ingredients as traditional concrete, the corresponding mix ratios are very different because RCC has no slump and contains less water and cement [2]. Its main advantage over traditional concrete applications is that it doesn't require surface finishing, steel reinforcement, or moulding. RCC is applied by layer-by-layer compaction using appropriate asphalt construction equipment or vibratory roller compactors [3]. Thus, it is imperative that the consistency of RCC is sufficiently desiccated to accommodate the load of a vibratory roller, while simultaneously possessing adequate moisture content to facilitate the uniform dispersion of the cement paste [4]. The cement hydration process has a major effect on the compressive strength of regular concrete, however in the case of RCC, both the compaction process and cement hydration have an impact on this component. The increased friction between the constituents of the concrete mixture as a result of compaction leads to an augmented loadbearing pressure and strength at the initial stage. It is imperative to achieve adequate compaction or density in order to attain the maximum strength values for RCC [5].

RCC are important not only for their strength but also for their durability [6]. The use of deicing salts and continuous freeze-thaw (F-T) cycles accelerate the deterioration of RCC structures, particularly in cold climates [7,8]. Concrete can incur various forms of deterioration, such as the occurrence of cracks and surface scaling, due to detrimental mechanisms. The capacity of a cementitious substance to withstand freeze-thaw cycles is largely contingent upon factors of the maximum distance between the paste and free surface, permeability, the quantity of water capable of freezing, and the extent of paste saturation [6]. In the instance of roller-compacted concrete, it is anticipated that there will be lower permeability, a reduced level of paste saturation, and a diminished presence of freezable water. This is attributed to the fact that RCC exhibits lower water content and a denser composition when contrasted with conventional concrete. Consequently, it follows that the resistance of RCC under F-T cycle is also seems to be similar to or surpass that of normal concrete [7].

According to Hazaree et al [9], it was observed that mixtures containing less than 150 kg/m³ of cement experienced failure after 100 freezing-thawing cycles. However, as the water to

cement ratios decrease and the cement content increases, the resistance to F-T cycles significantly enhances. The number of tolerated F-T cycles in the experimental investigation with even larger cement incorporation may be difficult to estimate and may not function well. The research conducted by Delatte and Storey [10] demonstrated that the amount of cement paste and the water to cement (w/c) ratio in the concrete have the most effects on the durability of F-T, rather than the level of compaction attained through the use of the gyratory compactor. The splitting tensile strength of samples plays a crucial role in determining the durability of RCC subjected to frequent freeze-thaw (F-T) cycles. This strength is closely intertwined with the adhesion between the aggregates and the cement paste, thereby exerting a significant influence on the overall durability of RCC. The w/c ratio and density are among the factors that impact the durability of the concrete. Siamardi and Shabani [11] conducted a study to investigate how micro-synthetic fibre affects the mechanical properties of non-air-entrained RCC under F-T cycles. Their findings indicated that the mass loss after subjecting the specimens to 300 F-T cycles was less than 5%. This result suggests that the specimens can be considered durable, as it falls within an acceptable threshold.

The physical and mechanical properties of RCC were examined by Rahmani et al [11] according which w/c ratio and cement content was varied from 0.3 to 0.55 and from 240 to 340 kg/m³, respectively. The findings indicated that a reduction in w/c ratio and a rise in the cement content had a positive impact on the physical and mechanical characteristics of RCC pavement. A distinguishing feature of RCC pavement is its low w/c ratio or its zero-slump characteristic. Therefore, these mixtures are affected by variations in the quantity of water and cement content (cementitious materials). The RCC should possess optimal dryness to minimize the extent of the roller sinking into the pavement, while also maintaining an adequate level of moisture to facilitate the dispersion of cement paste within the mixture during the processes of mixing, distribution, and compaction. The notion of reducing the w/c ratio in order to enhance strength may not yield the desired level of compaction. Thus, this perspective is deemed unfavourable; nevertheless, the determination of the w/c ratio is imperative in achieving the optimal combination of compressive strength and compaction simultaneously. The main objective of proportioning the ingredients in RCC is to create a balance that has a uniform mass and meets the necessary strength, durability, and permeability requirements for the intended application [4,9,12]. The use of supplementary cement materials to create environmentally friendly and cost-effective concrete has become more popular in recent years. As a result, numerous studies have been conducted in the concrete production industry to investigate cement substitution and alternative binder materials that can enhance the mechanical and durability characteristics [13– 15].

According to the understanding of literature, no studies to the authors' knowledge addressing the examination of the combined impact of nano-silica (NS) dosage and particle size on the

mechanical properties and durability of RCC have been found in the literature. This work addresses this significant practical aspect of RCC while taking into account uses of RCC including nano-silica that are exposed to cold weather; in these applications, the F-T resistance creates a common body of information relevant to this field of study. In this regard, the core objective of the present study is to explore the combined effect of particle size and the dosage of NS as a partial replacement of cement on the mechanical properties such as compressive and splitting tensile strengths and durability, including mass change, ultrasonic pulse velocity (UPV), and relative dynamic modulus of elasticity (RDME) after 150 F-T cycles for RCC mixes along with the microstructure analysis. Finally, the contribution of NS dosage and particle size as the independent variables on the mechanical properties and durability of RCC such as UPV, RDME and mass loss under F-T cycles is studied using analysis of variance (ANOVA). Ultimately, this study intends to contribute to the existing body of knowledge by providing a reliable, efficient, and cost-effective predictive model, artificial neural network, facilitating improved construction practices and material selection in cold-weather regions.

2. Experimental program

2.1. Materials

In this work, the water absorption and bulk specific gravity of the fine and coarse aggregates, possessing a nominal size of 10 and 20 mm were assessed. The measurements were carried out on river aggregates incorporated in each mixture, resulting in a water absorption of 3%-2.57 gr/cm³ for the fine aggregate and 2%-2.59 gr/cm³ for the coarse aggregate. The fine aggregate equivalent for combined aggregates was 78%, with a 3.8% passing percentage through sieve #200. According to ACI 325 [16], particle size distribution of mixed aggregates is illustrated in Figure 1. The properties included in Table 1 were the aggregate properties used in this research.

Portland cement type-II (ASTM C 150) was obtained from Neka cement plant, located in Mazandaran province, Iran, and used for preparing of RCC. SiO₂ nanoparticles, with a purity of 99.5%, in three distinct sizes, were supplied by US Research Nano-Materials Inc., Houston, USA (see Figure 2). Table 2 presented the chemical compositions of the cementitious materials along with its physical properties.

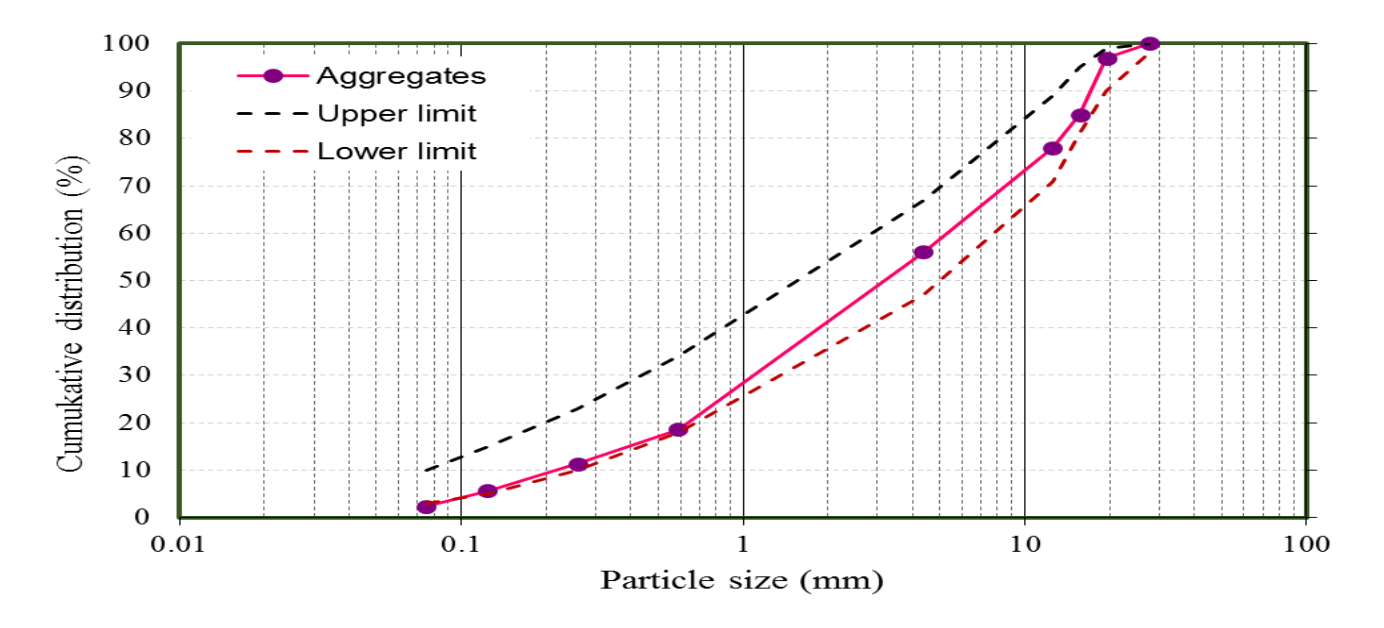


Figure 1. Grain size distribution of aggregates used for RCC mixtures.

Table 1. Physic	al properties o	f used	aggregates
-----------------	-----------------	--------	------------

Properties	Coarse aggregate	Fine aggregate
Apparent specific gravity	2.72	2.71
Density (OD) (kg/m ³)	2680	2609
Density (SSD) (kg/m ³)	2691	2644
Bulk density (kg/m ³)	1466	1493
Water absorption (%)	0.44	1.36
Los Angeles abrasion value (%)	13.98	-

Table 2. Chemical composition of utilized cementitious materials in percentage.

Component (%)	Cement	NS
SiO ₂	21.9	≥ 99
Al_2O_3	4.86	-
Fe_2O_3	3.3	-
CaO	63.32	-
MgO	1.15	-
SO_3	2.1	-

Na_2O	0.36	-
K_2O	0.56	-
Loss of ignition	2.4	0.2



Figure 2. The utilized NS with different particle size.

2.3. Mixture proportions

Table 3 contains information on the mix proportions of the RCC combinations. The first line is the mix percentage for the control RCC with OPC (no nano silica). The second set (lines 2-4) are RCC combinations with cement that has been partially replaced with NS 1% by weight of cement. The third group (lines 5–7) comprises of RCC mixtures in which cement is partially substituted with NS at a ratio of 3% by weight of cement. Similarly, the fourth group (lines 8–10) encompasses RCC mixtures where cement is partially substituted with NS at a ratio of 5% by weight of cement. Furthermore, the impact of varying particle size of NS, ranging from 8 to 30 nm, was examined within each group. The ratio of water to binder was consistently maintained at 0.41 for all mixtures. Furthermore, the quantity of binder, which consisted of type II Portland cement and NS, remained constant at 14% of the weight of the dry aggregate. This corresponded to a cement content ranging from 208 to 356 kg/m³ [17]. Four distinct groups were established based on the quantity and size of NS employed in each group. To illustrate, the designation RC1-D8 denotes a sample containing 1% NS with a particle size of

8 nm. These codes were utilized to present the specimens during the discussion of the experimental study and findings of the investigation.

Table 3. Mix proportions used to prepare RCC containing NS.

		Ingredient (kg/m³)						Size of NS	
Group	ID	Fine aggregate	Coarse aggregate	Water	Cement	NS	NS (%)	(nm)	
1	RC0	1165	855	121	295	0	0	0	
	RC1-D8	1165	855	121	292	2.9	1	8	
2	RC1-D15	1165	855	121	292	2.9	1	15	
-	RC1-D30	1165	855	121	292	2.9	1	30	
	RC3-D8	1165	855	121	286	8.8	3	8	
3	RC3-D15	1165	855	121	286	8.8	3	15	
-	RC3-D30	1165	855	121	286	8.8	3	30	
	RC5-D8	1165	855	121	280	14.7	5	8	
4	RC5-D15	1165	855	121	280	14.7	5	15	
-	RC5-D30	1165	855	121	280	14.7	5	30	

2.4. Casting procedure

Using the vibrating table, the specimens were compacted into three layers in compliance with ASTM C1176, procedure A. With the intention of achieving this objective, cylindrical specimens with a diameter of 150 mm and a height of 300 mm, as well as 150 mm \times 150 mm cube samples, were compacted by a surcharge weighing 9.1 kg. The specimens were subjected to a curing process under laboratory temperature conditions for a duration of 24 hours, and subsequently, they were protected by plastic covers. Following this, the specimens were extracted from their molds. Then, the samples were extracted from the mold and subsequently immersed in a water bath set at a controlled temperature of 23 \pm 2 °C until the age of 7 and 28 days in preparation for the evaluation of their mechanical characteristics. In order to attain more precise results, a total of three samples for each mix design were prepared, and the average values of each set were calculated accordingly for presenting the findings. Some images from the casting procedure and test setup is illustrated in Figure 3.

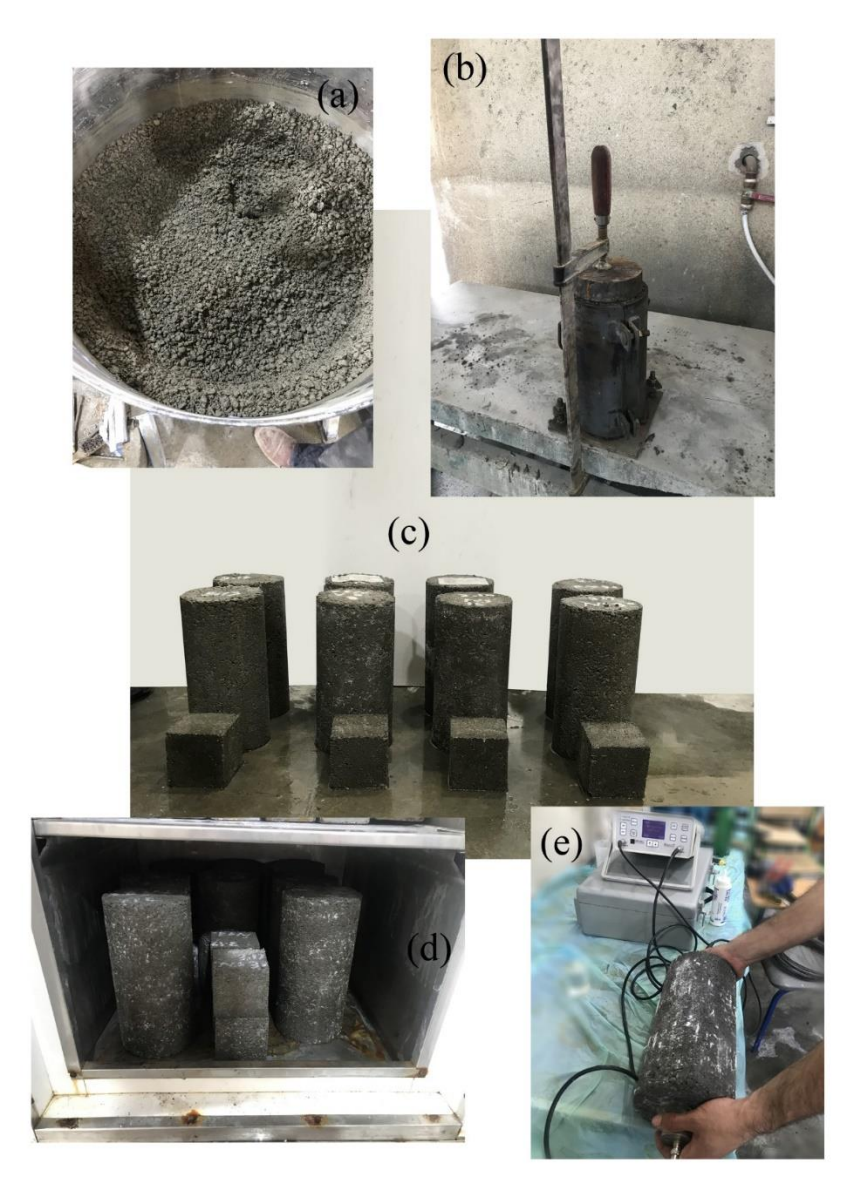


Figure 3. (a) Fresh RCC samples, (b) fixed cylindrical mold, (c) cylindrical and cube samples, (d) freeze—thaw test apparatus, and (e) UPV test.

2.5. Experimental methods

According to UNI EN 12390-3, a compressive test was performed on cube (150×150 mm) samples at 7 and 28 days of age to determine the compressive strength of RCC specimens [18]. To evaluate the splitting tensile strength, cylindrical specimens measuring 300 mm in height and 150 mm in diameter were examined in accordance with ASTM C496 [19].

The freeze-thaw resistance of RCCP specimens were evaluated according to ASTM C666 [20], procedure B. The specimens were placed inside a freeze-thaw chamber which had been

specifically designed for the purpose of freezing the samples at a temperature of -18 \pm 2 °C in presence of air and thaw them at a temperature of 5 \pm 2 °C in water. All RCC specimens underwent a total of 150 F-T cycles and for each 50 cycles the compressive strength was tested. In addition, in consecutive 50 cycles during the testing process some parameters such as mass loss, UPV and dynamic modulus of elasticity (E_{dn}) were measured and calculated to evaluate the durability of the proposed RCC mixes in each specific F-T cycle. The mass loss per unit surface area after every 50 freeze-thaw cycles is measured as follows.

$$M_{loss} = \frac{M_2 - M}{A} \tag{1}$$

Where, M_{loss} is mass loss, M_2 and M_1 are mass of sample after each complete 50 F-T cycle and at the beginning of the freeze-thaw cycle (zero cycle) in gram. In addition, surface area of the sample is representing by A. The RCC samples were tested for UPV values in accordance with ASTM C597 [21]. At the end of each consecutive 50 F--T cycle, the following equation is presented to calculate the E_{dn} .

$$E_{dn} = \rho c^2 \frac{(1+\vartheta)(1-2\vartheta)}{1-\vartheta} \tag{2}$$

Where ρ and c are density of RCC and UPV, respectively. Poisson's ratio (θ) is assumed to be 0.2. The water absorption test, conducted in accordance with ASTM C642 [22], involved the use of 150 mm cube samples of RCC.

The saturated surface dry weight (W_{ssd}) of the RCC specimens was determined, followed by drying the samples in an oven at 105 ± 5 °C for 24 hours until a constant weight was achieved. Subsequently, the water absorption ratio was obtained using the following equation based on the recorded mass (W_{ssd}).

$$WA = \frac{W_{ssd} - W_d}{W_d} \times 100 \tag{3}$$

3. Experimental results and discussion

3.1. Compressive strength

The results of the compressive strength test are depicted in Figure 4, showing that the inclusion of NS up to 3% led to an enhancement in the test outcomes when compared to those of the control RCC mixture. The inclusion of NS also played a role in the initial enhancement of the strength development of the RCC mixtures and the samples contain 1, 3, and 5% NS with 8 nm have an increment in 7 days compressive strength (23, 59, and 12%). This improvement is also observed for specimens with 15 and 30 nm with 1 to 5% NS is replaced with cement for constructing RCC. However, with upper than 3% NS (i.e., 5%) in this study, this can be resulted in lower improvement even with 1% NS replacement. The activity of NS particles is greater

than that of cement, allowing them to interact with CH crystals and produce C-S-H gel, thereby enhancing the density of concrete. The addition of an optimal quantity of NS can effectively improve the compressive strength of the concrete [23]. As a result of the enhanced filling effect and particle size distribution of nano particles, there has been a reduction in the porosity of concrete and an increase in their pozzolanic reaction with calcium hydroxide to produce CSH. Consequently, nano particles have garnered significant interest when compared to traditional mineral admixtures [24,25].

Based on research findings [23,26–28], the incorporation of a small amount of NS in concrete during its early stages has been shown to notably improve its compressive strength. The highest levels of compressive strength at early stages and after 28 days were achieved with a substitution rate of 2 to 3% of NS, suggesting that the most effective dosage of NS falls within this range [14,23,26,27]. Nano-silica facilitates the early-stage hydration of cement and exhibits a high pozzolanic activity, leading to the consumption and conversion of calcium hydroxide into CSH gel. This process ultimately improves the mechanical characteristics of the concrete [29]. Thus, the optimum NS content corresponding to the maximum compressive strength as can be seen from Figure 4, is 3% with same particle size.

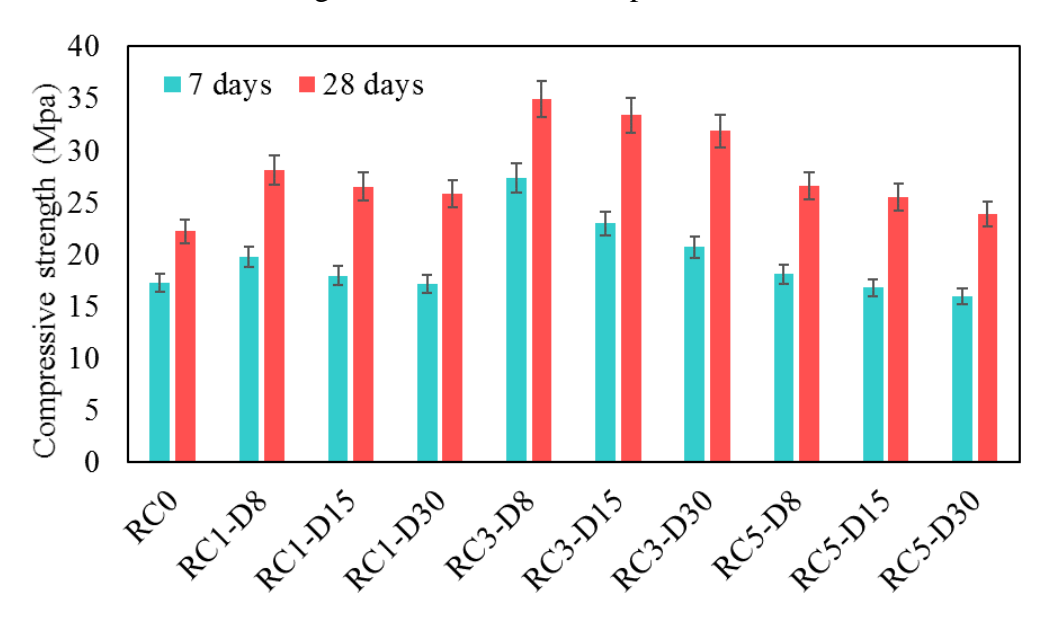


Figure 4. Test results of compressive strength of RCC specimens with different dosage and size of particle

In term of NS particle size, it can be observed from Figure 4 that RCC containing smaller particle size of NS, exhibited a higher strength in comparison to bigger particles, especially in early ages, which is proven in literature [26,30]. Compared to RCC with 15 and 30 nm NS particles, NS with 8 nm particle size could increase compressive strength by 6 and 9%.

3.1. Splitting tensile strength

The results of splitting tensile strength for RCC specimens containing NS particles at 7 and 28 days are displayed in Figure 5. The results indicate that the splitting tensile strength of control RCC was 2.37 MPa at 28 days. The splitting tensile strength of the RCC with 1, 3, and 5% NS with 8 nm particle size at 28 days improved by 21.5, 49.7, and 15.2%, respectively, relative to the control mix, thus, the optimum inclusion of NS in RCC mixes is determined as 3% replacement. In addition to the NS dosage, the particle size of this material can also play a great role as a partial replacement of cement in mixtures. As can be seen from the results, the splitting tensile strength of RCC specimens decreased when the particle size increased from 8 nm to 15 and 30 nm. For instance, the splitting tensile strength for RC3-D15 and RC3-D30 decreased by 11.26 and 20.56% compared to RC3-D8.

Moreover, the splitting tensile strength of the RCC samples incorporating NS exhibited an increase in comparison to the mixes without NS. This outcome was largely anticipated due to the similar factors previously discussed regarding the impact of NS on compressive strength. The NS enhances the microstructure of the cement matrix, consequently enhancing the bond between cement, aggregate, and interfacial transition zone (ITZ), which is likely responsible for the observed improvement in splitting tensile strength [31]. The highest increase in splitting tensile strength was for RCC containing 3% NS with 8 nm particle size and this mix, RC3-D8, show better bond between aggregate and cement paste.

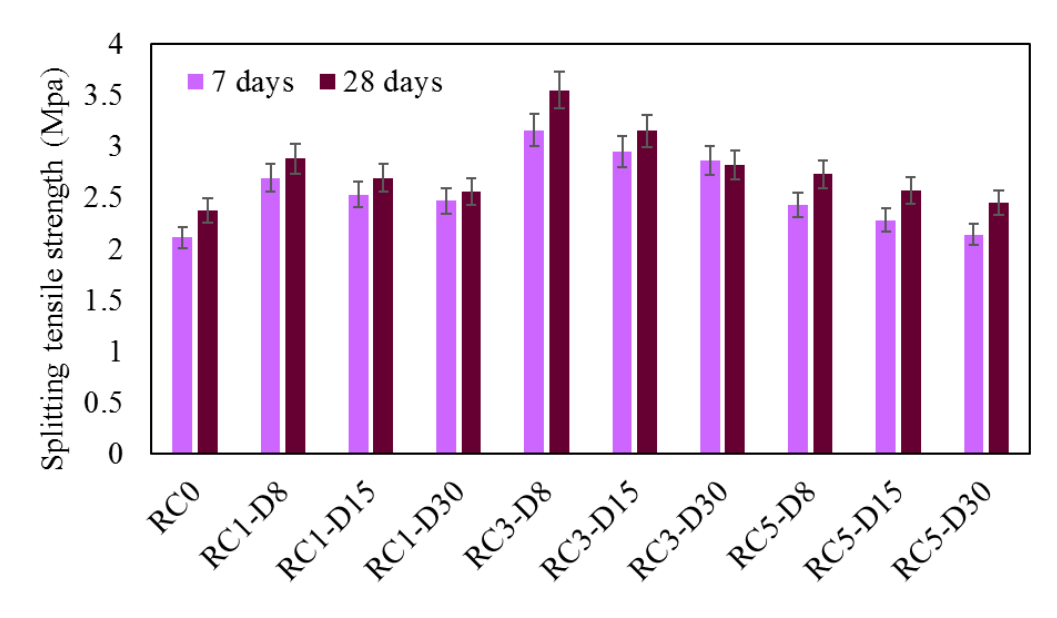


Figure 5. Test results of splitting tensile strength of RCC specimens with different dosage and size of particle

The relationship between compressive strength and splitting tensile strength of RCC containing NS with different dosages and particle sizes is shown in Figure 6. The findings of this study indicate there is similar pattern in the trends of compressive and splitting tensile strengths. Specifically, the splitting tensile strength of the RCC samples was approximately $11 \pm 0.86\%$ of the compressive strength. This suggests that the splitting tensile strength to compressive strength ratio of the RCC is relatively higher compared to that of traditional concrete, according which the ratio for normal concrete with the range of 35.1-51.1 MPa of compressive strength is usually below 10% [32]. In addition, a regression-based equations was presented by Chhorn et al. [33] and Rahmani et al. [11] on the relationship between the compressive and splitting strengths. They found that power equation (Eqs. (4) and (5)) among the different types of linear regression equations yielded the best results.

$$f_{st-Chhorn\,et\,al.} = 0.47 f_c^{\ 0.511}$$
 (4)

$$f_{st-Rahmani\ et\ al.} = 0.69 f_c^{0.5} \tag{5}$$

where f_{st} and f_c are the splitting tensile and compressive strengths (MPa), respectively.

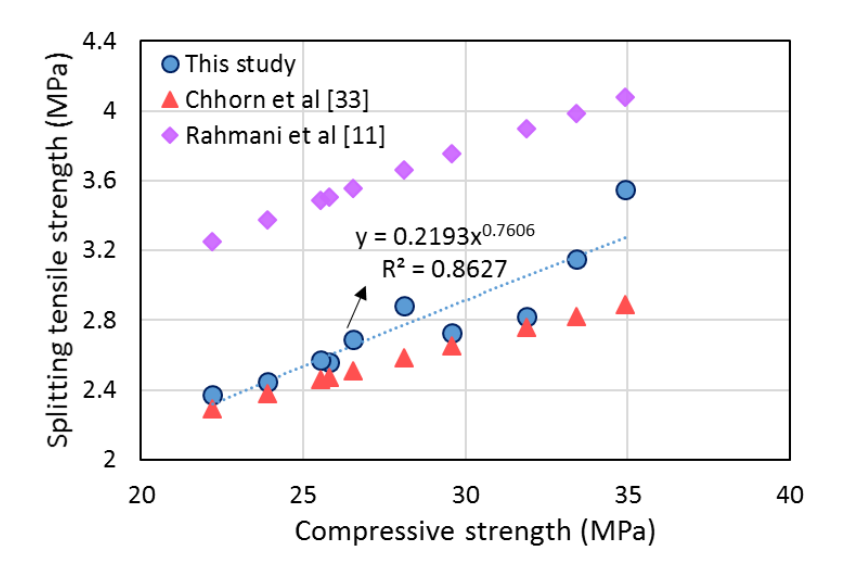


Figure 6. Relationship between compressive strength and splitting tensile strength of RCC containing NS at 28 days.

3.2. Water absorption

The water absorption values of RCC as well as the standard deviation values is presented in Figure 7. As shown in Figure 7, the water absorption generally reduced by adding NS into the RCC mixtures which was proven by previous studies [15,34–36]. The water absorption rates

of the RCC specimens vary between 3.28% and 5.27% at 28 days, and RC5-D8 had the minimum test results. It was also observed that by using greater NS particle size of 8 nm to 15 and 30 nm in RCC mixtures with constant dosage, the water absorption increased from 3.72% to 4.05 and 4.28%, respectively.

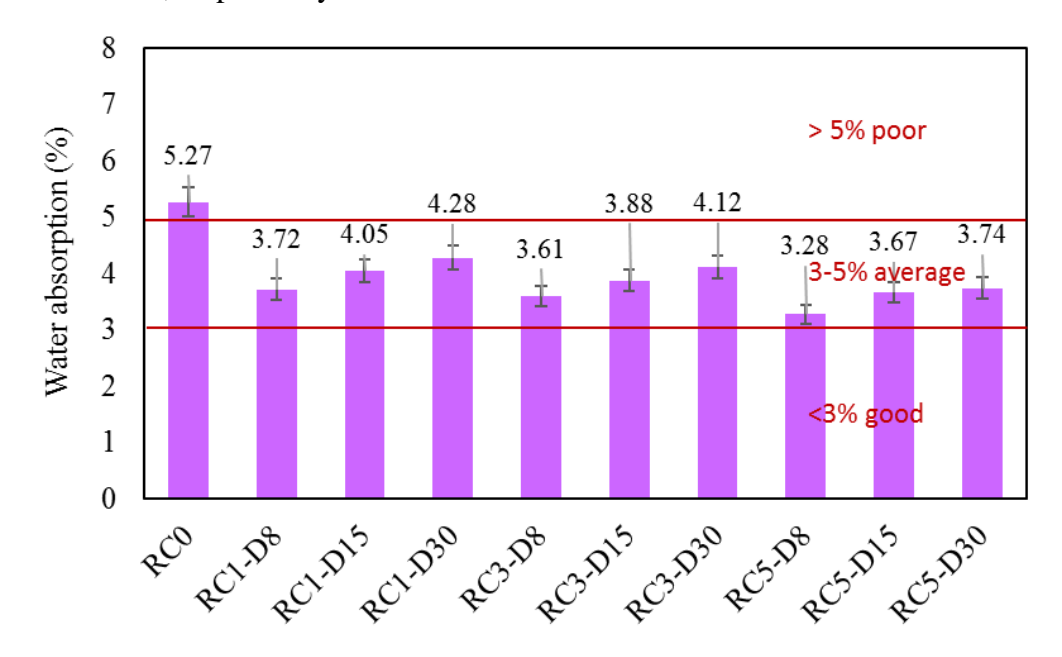


Figure 7. Water absorption values of RCC specimens

Furthermore, at the same NS particle size of 8 nm, the inclusion of 5% NS reduced water absorption more significantly compared to 3% and 1% inclusions by 0.44 and 0.33%, respectively. The reduction in water absorption may be due to the high reactivity of NS by forming more CSH gel and filling the voids of the concrete matrix, and thus increasing the pore size distribution. As a result of the filling and strong pozzolanic effects of NS particles, the threshold pore diameter in RCC was decreased, leading to a notable increase in the proportion of small pores (micro-cracks). This effect was particularly pronounced when NS particles of 8 nm were used at a dosage of 5%, as compared to lower dosages and larger particle sizes [37].

The proposed correlation between the water absorption and compressive strength of the RCC incorporating NS is illustrated in Figure 8. This relationship was found to be inversely proportional. In other words, the RCC mixture's durability and compressive strength increased as its permeability decreased. This phenomenon can be attributed to the higher porosity and void content in the RCC, which could result in stress concentration and the formation of micro cracks under applied loads. Consequently, this could lead to premature failure and a subsequent decrease in compressive strength [38].

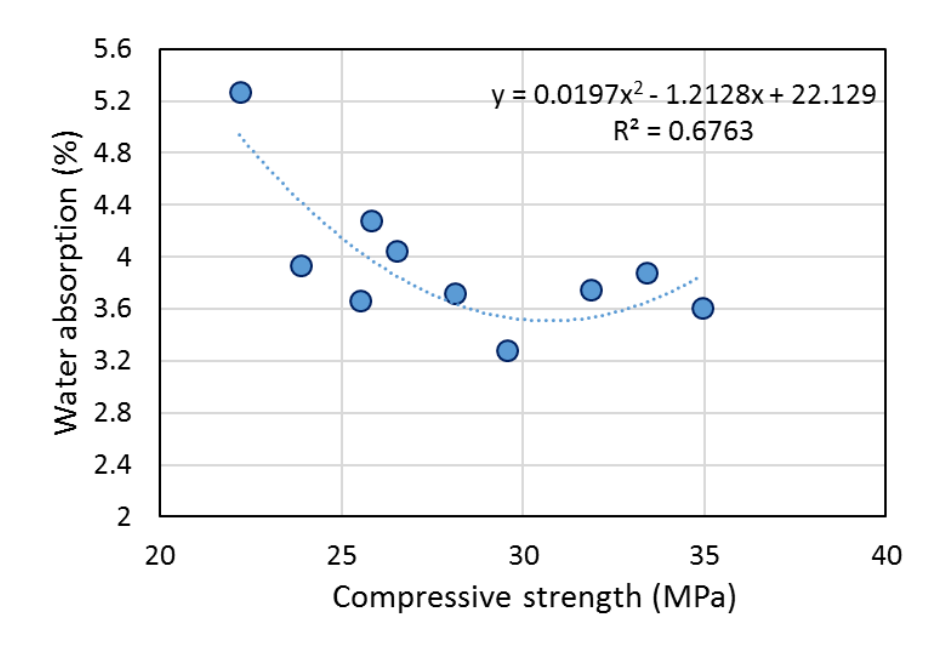


Figure 8. Variation of water absorption vs. compressive strength for RCC mixes containing NS particles.

3.3. F-T resistance test

3.3.1. Ultrasonic Pulse Velocity (UPV)

The findings of the UPV test after 150 consecutive freeze-thaw cycles are depicted in Figure 9. The decline in UPV correlates with the escalating number of F-T cycles, as the advancing F-T cycles lead to a slight augmentation in the pore structure of the RCC containing NS. As per existing literature, RCC mixes with UPV values below 2 km/s, between 2-3.5 km/s, between 3.5-4.5 km/s, and exceeding 4.5 km/s, respectively, are classified as poor, acceptable, good and strong concrete [1]. Therefore, the RCC specimens with and without NS particle can be categorised as acceptable before exposing to F-T cycles. Based on Figure 9, after 150 F-T cycles, the reduction in UPV for the mixes containing 3% NS was the least in all three groups of particle size. The RCC with 5% NS showed the worst performance, changing from 4.495 km/s (initial) to 4.011 km/s (150 cycles) compared to those incorporating NS. It is noteworthy that the trend of decreasing UPV value after 150 F-T cycles did not change when the particle size of NS varied from 8 nm to 15 and 30 nm and just insignificantly decreased. In addition, the decrease in UPV for mixes containing 1 and 5% NS is quite close to each other approximately in all F-T cycles with different NS particle size.

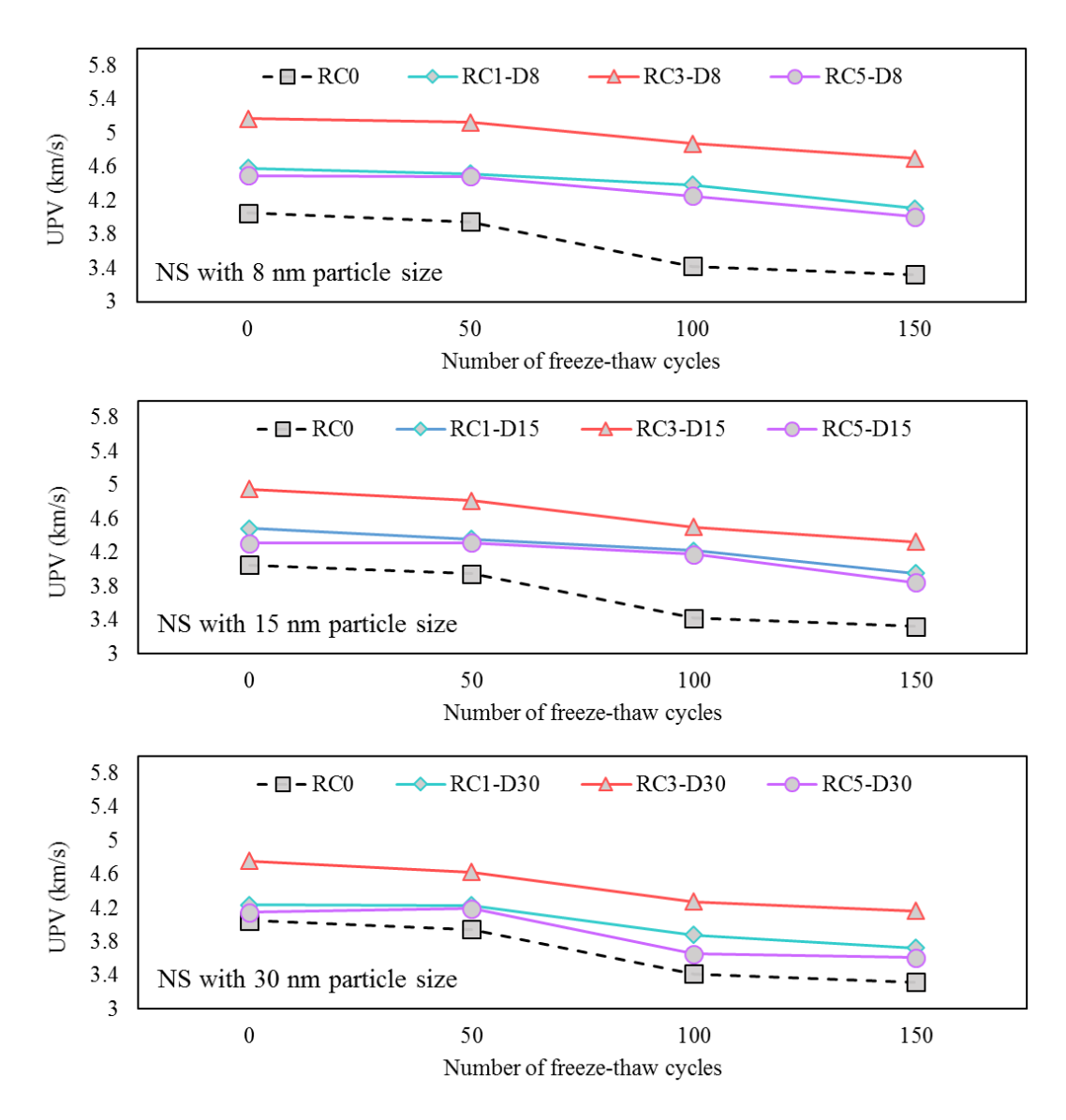


Figure 9. UPV results test for RCC containing NS with 8, 15, 30 particle size after conditioning in freeze-thaw cycles

3.3.2. Relative Dynamic Modulus of Elasticity (RDME)

Figure 10 shows the variations of the RDME with the number of F-T cycles. It can be seen from the results, after 100 cycles, the RCC mixtures containing NS had RDME over 85% and after 150 cycles, the RDME was decreased by about 3%. RCC mixes containing 5% NS were more vulnerable to freeze-thaw cycles than the inclusion of 1 and 3% NS. According to the results, in the group of RCC mixtures which NS was partially added 5%, RCC5-D8 experienced higher percentage of RDME (92.65%) after 150 cycles compared to RCC5-D15 and RCC5-D30 with RDME of 87.97 and 86.26%, respectively.

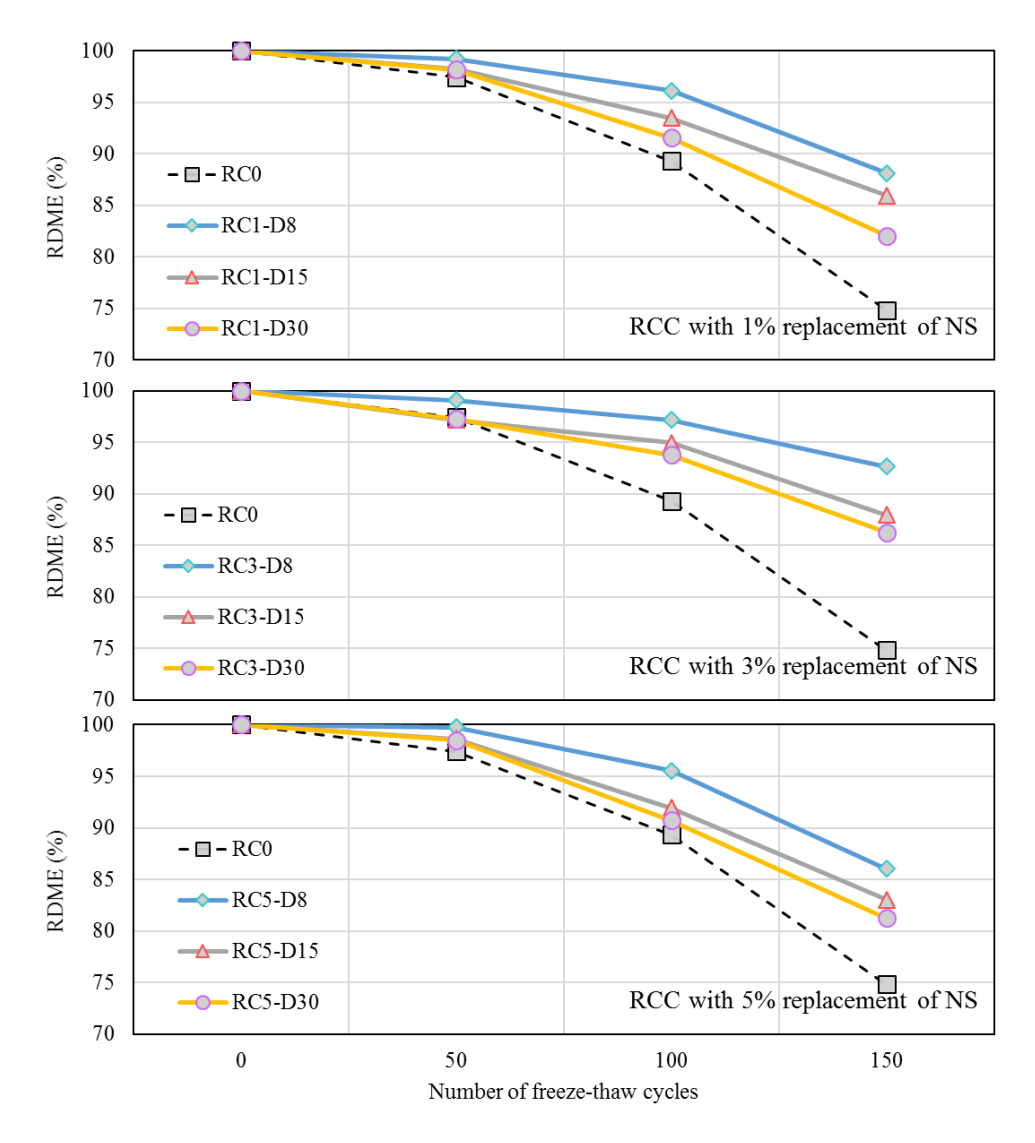


Figure 10. RDME of RCC containing NS with different dosage after conditioning in freeze-thaw cycles

3.3.3. Changes in mass

Figure 11 illustrates the mass loss of the RCC containing NS after consecutive freeze-thaw cycles. Three parallel specimens were tested for each mixture, and the averaged results are calculated to present. The data in Figure 11 indicates that as the freeze-thaw cycles progress, the mass loss values increase, with the RCC incorporating NS exhibiting lower mass loss compared to the control samples. However, the mass loss differences between the RCC sample results correspond to the NS contents in terms of dosage and particle size. As can be seen from the results, the lowest mass changes (2.61%) after 150 cycles is related to RCC specimens.

containing 3% NS with the particle size of 8 nm. This value for specimens containing same dosage of NS with 15 and 30 nm is calculated 3.58 and 4.63%.

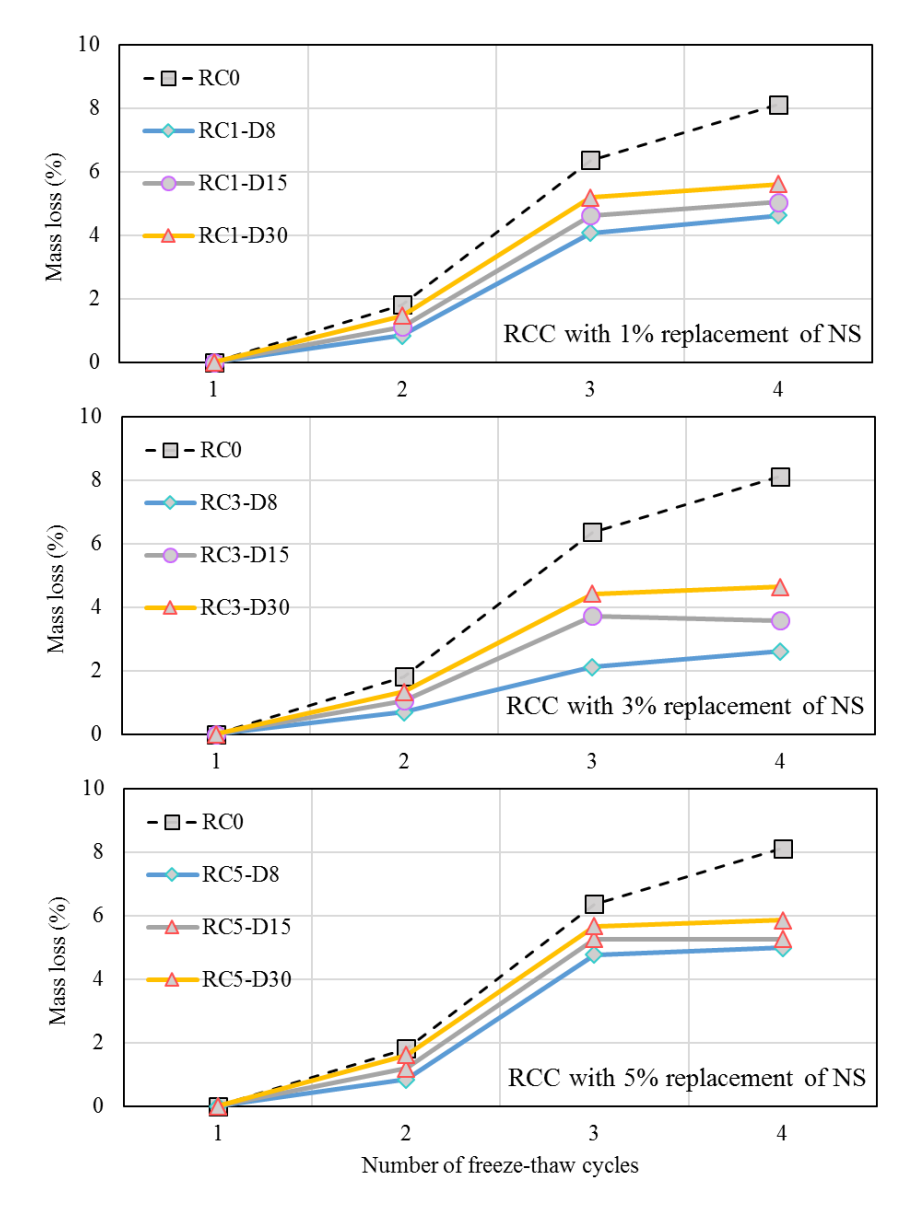


Figure 11. Mass loss of RCC containing NS with different dosage after conditioning in freeze-thaw cycles

3.4. Microstructure study

Figure 12 exhibits SEM micrographs of RCC specimens containing 0, 1, 3, and 5% NS with the same 8 nm particle size. The structure of RCC incorporating NS is very similar to the control RCC matrix and its microstructure of the interfacial zone is clearly dense and uniform.

By comparing the microstructures of RCC specimens, it was determined that nano silica not only served to occupy the empty spaces amidst the particles within the concrete structure but also facilitated the chemical process and initiated the production of C-S-H gel to occupy the voids within the concrete mixture. Based on Figure 12, SEM of RCC without NS as the reference sample reveals a notable presence of porosity, microcracks, C-H, C-S-H, and most of the unreacted material, which can be attributed to an excessive cement content. It can be seen from the SEM of RCC specimens containing different dosages of NS that the size of the pores and C-H crystals is reduced, creating a microstructure that is extra compressed when the inclusion of NS is increased.

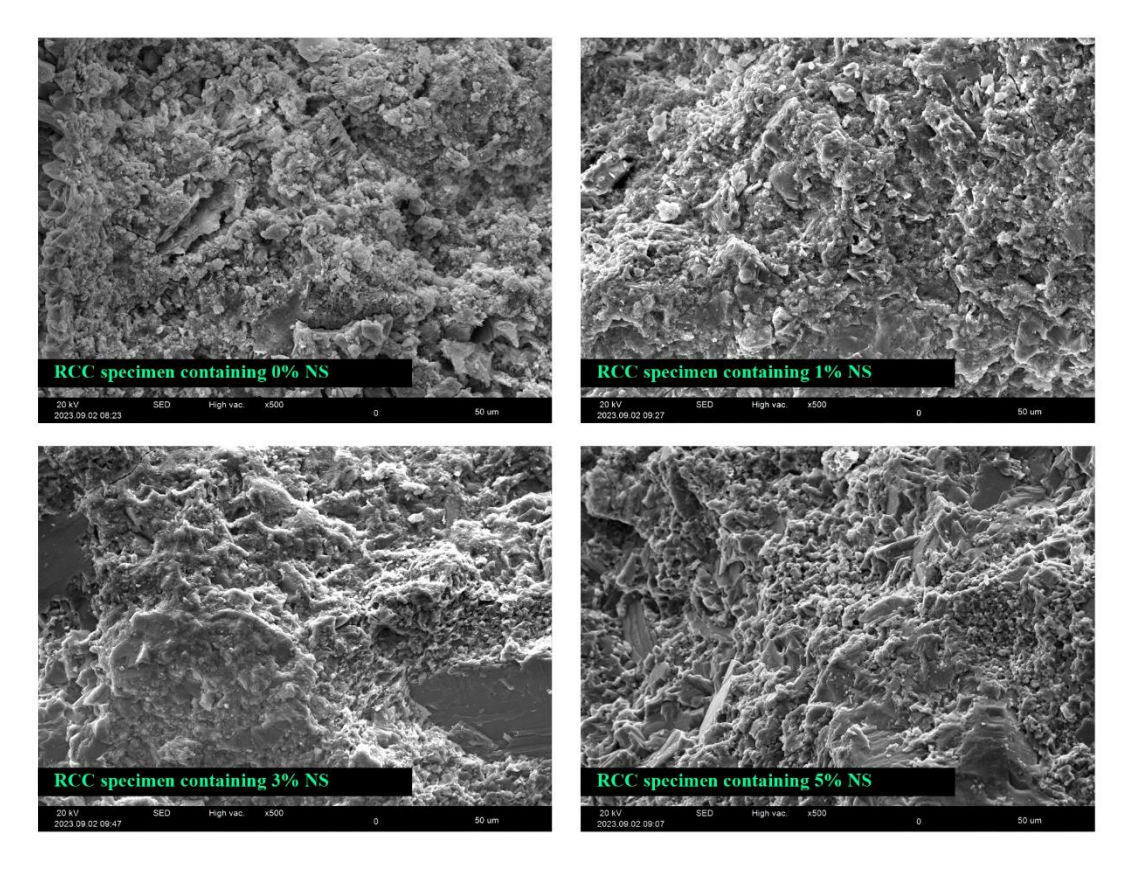


Figure 12. SEM micrographs of roller compacted concrete incorporating 0, 1, 3, and 5% nano-silica with 8 nm particle size.

3.5. Statistical analysis by analysis of variance

In this study, the contribution of independent parameters such as dosage and particle size of nano-silica in the concrete compressive strength is investigated by analysis of variance (ANOVA) [39–41]. The input variables are dosage and particle size of nano silica. The ANOVA results for the compressive and splitting tensile strengths along with UPV, RDME, and mass loss for all RCC samples under different F-T cycles are shown in Table 4. The high

variance values indicate that the examined parameters exerted a substantial impact on the performance of the RCC mixes. The findings show that the dosage of NS had a major influence on the properties, with percent contributions of 81.74, 60.57, 82.65, 94.46 and 83.98% for the compressive strength, splitting tensile strength, UPV-150, RDME-150, and mass loss-150, respectively. These observations indicate that the percentage replacement of NS was a more influential factor compared to its particle size for all mechanical properties and durability factors.

Table 4. Results of ANOVA for the mechanical properties and durability of RCC under freeze-thaw test

Experimental factors	DF	SS	Var	P-value	Contribution (%)			
Compressive strength (MPa)								
Particle size of NS (nm)	3	9.93	3.317	0.187	14.37			
Dosage of NS (%)	3	56.61	18.871	0.133	81.74			
Error	6	5.34	0.899	0.079	3.89			
Total	12	71.88	23.088	-	100			
	S	plitting tensile	strength (MP	a)				
Particle size of NS (nm)	3	0.133	0.044	0.181	29.22			
Dosage of NS (%)	3	0.276	0.092	0.151	60.57			
Error	6	0.09	0.015	0.079	10.21			
Total	12	1.368	0.152	-	100			
		UPV-150) (km/s)					
Particle size of NS (nm)	3	0.164	0.054	0.198	16.76			
Dosage of NS (%)	3	0.809	0.269	0.155	82.65			
Error	6	0.011	0.002	0.079	0.60			
Total	12	2.939	0.326	-	100			
		RDME-1	50 (%)					
Particle size of NS (nm)	3	3.635	1.211	0.257	2.38			
Dosage of NS (%)	3	144.195	48.065	0.123	94.46			
Error	6	9.635	1.605	0.079	3.16			
Total	12	457.941	50.88	-	100			
Mass loss-150 (%)								
Particle size of NS (nm)	3	1.315	0.438	0.21	12.97			
Dosage of NS (%)	3	8.518	2.839	0.152	83.98			
Error	6	0.61	0.103	0.079	3.05			
Total	12	30.431	3.381	-	100			

3.6. Establishment and validation of artificial neural network

3.6.1. ANN description

The principles of the artificial neural network (ANN) were originally developed based on the biological neural structures found in animal brains, aiming to address a wide array of complex problems in the previous century [42]. The structure of the ANN consists of three layers: the input layer, hidden layer, and output layer. The input layer can have at least one input element, generating raw output data. In the hidden layer, inputs are manipulated through various operations, with its design and purpose varying based on the network's configuration, which can be either single-layered or multi-layered. The output layer includes at least one output whose value is determined by the network's function. This layer carries out computations and sends its results to the external environment [43–45]. The model described can incorporate multiple basic functions for the hidden layer. In regression scenarios, a linear function is typically used for the output layer. It's important to highlight that the regression function approximated by the ANN can be represented uniformly, regardless of the particular hidden basic function utilized [46]:

$$f(x,W,\beta) = \beta_0 + \sum_{j=1}^m \beta_j B_j(x,w_j)$$
(6)

where $B_j(x, w_j)$ stands for the set of non-linear transformations of the input vector $x^T = (x_1, x_2, ..., x_d)$, where $x^T \in R^d$; a bias term, β_0 , is considered; $\beta^T = (\beta_1, \beta_2, ..., \beta_m)$ are the coefficients from the hidden layer to the output layer; $W^T = (W_{j1}, W_{j2}, ..., W_{jd})$ are the parameters from the input layer to the j-the hidden node, and finally, m is the number of basis functions or hidden neurons of the model. Through utilization of predetermined weight values during the process cycle, the training gradually evolves. The progress is evaluated by assessing the expected outcome against the actual result, and then adjusting error values to adjust weights and reduce overall errors. A predetermined parameter can also be used as the model and pattern threshold. Furthermore, a slight bias can be incorporated into the input data output to establish decision boundaries and pattern thresholds. The choice of activation function depends on the complexity of the problem being addressed. In cases involving nonlinear problems, Sigmoid functions like log-sigmoid or tangent sigmoid are often utilized.

3.6.2. Database and model parameters

The database employed in constructing the ANN model comprises the findings from mechanical properties and durability tests conducted on RCC samples subjected to different numbers of F-T cycles. A total of 30 datasets were utilized to predict the compressive strength under F-T cycles, aiming to analyze the impact of these cycles on RCC's mechanical properties. Three key parameters from the experimental tests - UPV at zero F-T cycle (UPV0), number of F-T cycles (NFT), and specimen mass (M) - were designated as input variables for the ANN

model. Consequently, the compressive strength of RCC containing nano-silica under F-T cycles was expressed as a function of the following parameters:

$$CS = f(UPV_0, NFT, M) \tag{7}$$

A primary issue in constructing the ANN model is the problem of overfitting. This situation arises when the model shows strong performance on the training data but struggles with new testing data, resulting in increased errors. To address this challenge, researchers recommend splitting the database into separate training and testing datasets [47]. Training data is utilized for building and adjusting the model, while testing data is used to assess the effectiveness of the model on unseen data that was not part of the initial development process [48]. It is suggested that 75% and 25% of the data are sufficient for training and testing the developed models, respectively.

It is crucial to use an adequate number of datasets during model development to ensure the reliability of the models. To create a dependable and secure model, it is suggested that the ratio of datasets to variables should exceed 5 [49]. In this study, this ratio is equal to 30/3 = 10, which indicates that the number of datasets is sufficient for modelling the investigated problem.

3.6.3. Performance analysis

In the present study, the proposed models were assessed by means of various performance measures (Eqs. (8)- (10)). The measures of precision and error employed in this study encompassed the correlation coefficient (R), root mean square error (RMSE), and mean absolute error (MAE). These metrics were expressed as follows.

$$R = \frac{\sum_{i=1}^{N} (T_{obs} - \overline{T_{obs}}) \cdot (T_{pre} - \overline{T_{pre}})}{\sqrt{\sum_{i=1}^{N} (T_{obs} - \overline{T_{obs}})^2 \sum_{i=1}^{N} (T_{pre} - \overline{T_{pre}})^2}}$$
(8)

$$RMSE = \sqrt{\frac{1}{N} \sum_{i=1}^{N} \left(T_{pre} - T_{obs} \right)^2}$$
 (9)

$$MAE = \frac{\sum_{i=1}^{N} |T_{pre} - T_{obs}|}{N}$$
 (10)

where T_{obs} and T_{pre} are the observed and predicted values, respectively; $\overline{T_{obs}}$ and $\overline{T_{pre}}$ represent the mean of the observed and predicted values, respectively; and N is the number of data. Table 5 provides a summary of the performance of the advanced ANN model with both training and testing data. The results indicate that the ANN model demonstrated satisfactory predictive capabilities for compressive strength. Key statistical parameters for the model include an R-value of 0.98, RMSE of 0.706 MPa, and MAE of 0.484 MPa for training data, as well as an R-value of 0.97, RMSE of 1.033 MPa, and MAE of 0.943 MPa for testing data.

Table 5. Performance evaluation of developed ANN model for compressive strength of RCC under F-T cycles.

	R	RMSE	MAE	
Training stage	0.98	0.706	0.484	
Testing stage	0.97	1.033	0.943	

During the training and testing phases, the agreement between the observed and projected compressive strength of RCC was evaluated visually using scatterplots (Figure 13a). The assessment revealed a high degree of accuracy in replicating the compressive strength of RCC under F-T cycles using the ANN model in both phases. Additionally, a line graph (Figure 13b) was used to demonstrate the predictive results and fluctuations in a range of experimental compressive strengths, with a focus on outliers.

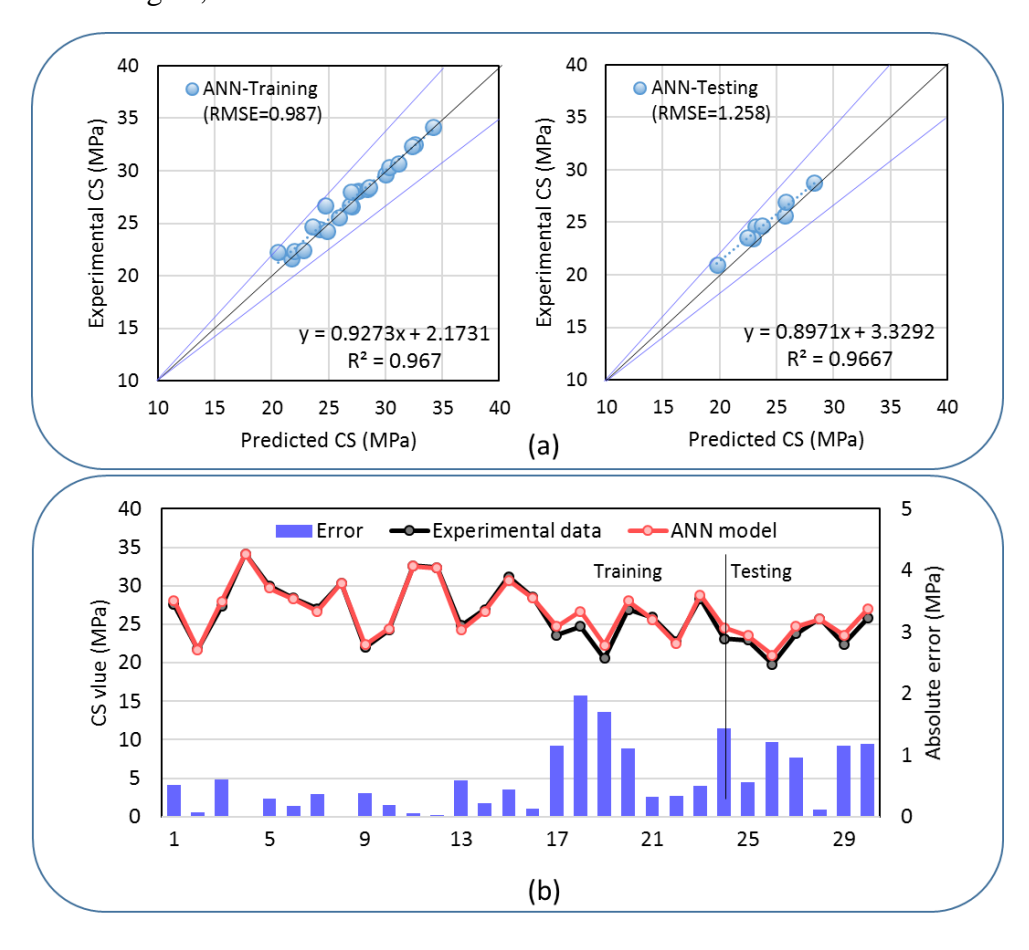


Figure 13. Comparison of observed vs. predicted compressive strength of ANN model a) scatter plots b) line graph with absolute error.

Based on this data, the ANN model demonstrated greater precision in replicating experimental outcomes during the training phase than during the testing phase. Moreover, its absolute error was consistently minimal when forecasting the compressive strength of RCC. Additionally, a supplementary evaluation of the ANN model was carried out to investigate the impact of individual input variables on compressive strength under F-T cycles.

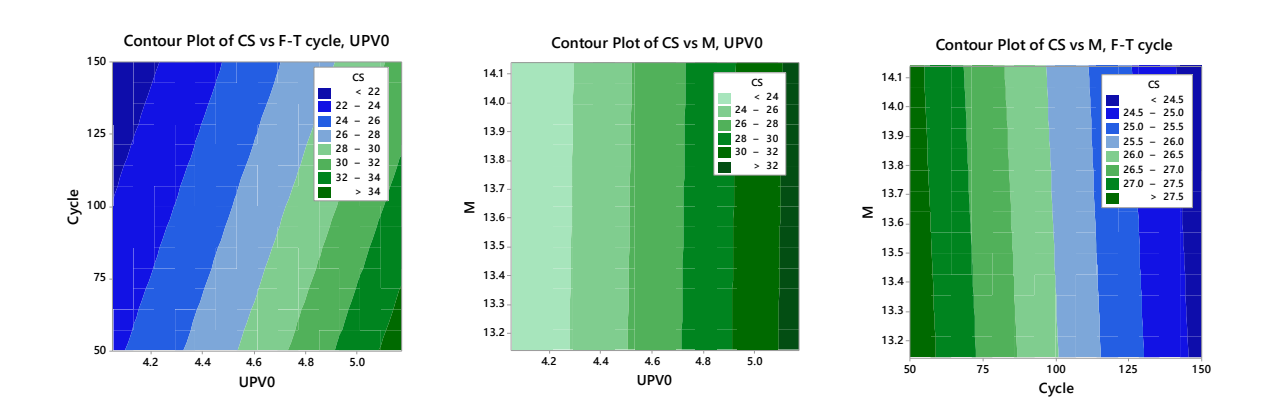


Figure 14. Contour plots of compressive strength vs. NFT, UPV₀, and M for RCC.

The artificial neural networks operate by utilizing the known weights and bias values across various layers. In contrast to prior research focusing solely on optimizing network structure, this study presents the weights and bias values for each layer of the ANN model in Table 6 to facilitate easy replication of results. Through these provided values, one can directly calculate the compressive strength for RCC using common spreadsheet software. The suggested model is defined by the specific weights and bias obtained from the ANN model. The relationship between normalized input parameters (NFT, UPV0, M) and compressive strength (CS) is expressed through a mathematical equation as follows:

$$CS = f\{b_0 + \sum_{k=1}^{h} [w_k f(b_{hk} + \sum_{i=1}^{m} w_{ik} X_i)]\}$$
(11)

where f is the transfer function, h indicates hidden layer neuron numbers, X_i indicates the normalized values of network input, m is the number of the input variables, w_{ik} indicates the linking weights between the ith input and kth neuron in the hidden layer, w_k is the link weight between the kth neuron in the hidden layer and the independent output neuron, b_{hk} shows the bias in the kth neuron of the hidden layer and k0 is the bias value in the output layer. For the presented weights in Table 6 and Eq. (12), the bond strength relation between the FRP composite and the concrete substrate can be as follows.

$$CS = -1.685A1 + 0.8527A2 - 0.5721 - 0.3684 + 0.0553$$
 (12)

where A_i , (i = 1 to 4) are hidden neuron responses that feed the network output value and can be calculated with the following equation:

$$\begin{bmatrix} A1\\ A2\\ A3\\ A4 \end{bmatrix} = tansig(\begin{pmatrix} \begin{bmatrix} -0.5067 & -0.9312 & 1.8764\\ 0.9223 & -0.4426 & -0.0785\\ 2.0961 & 0.3589 & -0.4473\\ -1.9237 & 0.7237 & -0.7684 \end{bmatrix} \begin{bmatrix} UP0\\ NFT\\ M \end{bmatrix}) + \begin{bmatrix} -1.685\\ -0.455\\ 1.4018\\ -2.8046 \end{bmatrix})$$
 (13)

Table 6. The weights and bias values of the ANN model for the prediction of compressive strength of RCC under F-T cycles.

Number		We		Bi	as	
of	W _{ik}		V V.	b	h.	
neurons	UPV_0	NFT	M	\mathbf{W}_{k}	b_{hk}	b_0
1	-0.5067	-0.9312	1.8764	-1.685	2.4583	
2	0.9223	-0.4426	-0.0785	0.8527	-0.455	0.0553
3	2.0961	0.3589	-0.4473	-0.5721	1.4018	0.0333
4	-1.9237	0.7237	-0.7684	-0.3684	-2.8046	•

3.7. Shapley additive explanations (SHAP)

The SHAP Analysis, as proposed by Lundberg and Lee [50], offers a detailed methodology for understanding ML models. It introduces the concept of SHAP, which provides a unified way to interpret models. The Shapely value is employed to illustrate the relative influence of individual input variables on the final output variable. This approach is akin to parametric analysis, where all variables except one are held constant to observe the impact of the variable in question on the target attribute. The model generates predicted outcomes for each expected sample, with the SHAP value indicating the significance assigned to each feature within that sample [51].

The study investigated how input parameters affect the compressive strength of RCC including nanoparticles during F-T cycles. Using the SHAP explainer, a comprehensive analysis was conducted to show localized SHAP explanations and overall feature impact. The SHAP plot in Figure 15 illustrates the effects of input factors on RCC compressive strength, with each element's value depicted through colors and the x-axis SHAP value indicating each factor's influence. The most significant factor influencing RCC compressive strength was identified as UPV at zero cycle, showing a strong correlation. The results suggest a direct link between UPV0 values at zero cycle and RCC CS, implying that increasing UPV0 proportion in the mix

enhances RCC compressive strength. Positive correlations were also observed for mass and cycle numbers based on the SHAP plot analysis.

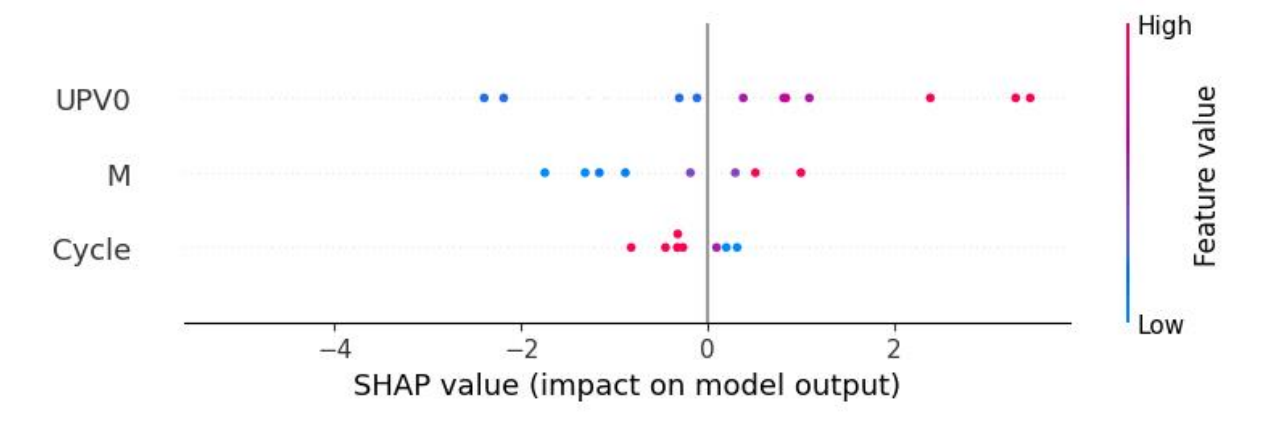


Figure 15. SHAP plot for the relevance of input features on compressive strength under F-T cycles.

To provide a detailed explanation and interpretation of the forecasted compressive strength during F-T cycles, we illustrated and clarified an individual breakdown of the model's prediction utilizing a force chart, as depicted in Figure 16. This chart represents the prediction for a specific RCC sample, incorporating varied values of UPV0, M, and NFT cycle. The function f(x) denotes the model's output (the anticipated probability for the given sample), with the base value reflecting the average of model predictions. Features that increase (increase) the prediction are depicted in red, while those that reduce (decrease) it are shown in blue. Furthermore, red features are indicated by right arrows, whereas blue features are denoted by left arrows, with arrow size indicating feature impact.

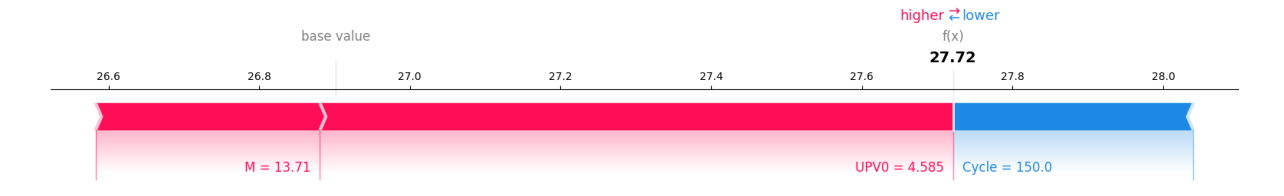


Figure 16. SHAP force plot for predicting compressive strength under F-T cycles.

4. Conclusion

In this study, the addition of nano-silica as the partial replacement of cement was examined in terms of dosage and particle size, focusing on its effects on the mechanical properties and

durability of the RCC. For this purpose, nano silica replaced cement at 1%, 3% and 5%. In addition, the coupling effects of the dosage and particle size of nano-silica with 8, 15, and 30 nanometres were also investigated. Compressive and splitting tensile strengths, water absorption along with mass loss, ultrasonic pulse velocity, and dynamic modulus of elasticity under freeze-thaw test were conducted. The following findings were drawn:

- Compressive strength of RCC increased from 12 to 59% at 7 days of curing when nanosilica was used as the partial replacement of cement. Furthermore, by increasing the particle size of 3% NS from 8 nm to 15 and 30 nm, the compressive strength decreased by 4.3 and 8.7%. With an increase in the NS dosage from 1% to 3%, the splitting tensile strength of RCC raised from 2.88, 2.69, and 2.56 MPa to 3.55, 3.15, and 2.82 MPa, respectively, for 8, 15, and 30 nm NS particle size.
- It was observed that using NS with the particle size of 8 nm to 15 and 30 nm in RCC mixtures with constant dosage, 3%, the water absorption increased from 3.72% to 4.05 and 4.28%, respectively. In addition, the RCC specimen with 5% NS inclusion and 8 nm particle size had the lowest water absorption rates.
- The reduction in UPV for the mixes containing 3% NS was the least in all three groups of particle size after 150 freeze-thaw cycles. The RCC with 5% NS showed the worst performance, changing from 4.495 km/s (initial) to 4.011 km/s (150 cycles) compared to those incorporating NS.
- The RDME values decrease as the freeze-thaw cycles progress. The decrement for RCC mixes containing 3% NS is about 7.35, 12.03, and 13.74%, respectively, with 8, 15, and 30 nm particle size after 150 cycles. Accordingly, RCC mixes containing 5% NS were more vulnerable to freeze-thaw cycles than the inclusion of 1 and 3% NS.
- The RCC with added NS has lower mass loss values compared to the control RCC because the inclusion of NS reduces water ingress and in consequence decreases water absorption.
- ANOVA analysis revealed that nano silica dosage was a more effective parameter than the its particle size in all experiments.
- The ANN model's development demonstrates its high reliability in predicting the compressive strength of RCC under F-T cycles based on factors such as the number of F-T cycles, UPV values in normal conditions, and sample mass.
- This study introduces the SHAP method to enhance the interpretability of machine learning outcomes. This technique generates detailed visualizations of feature attributions, enabling a better understanding of gold price fluctuations. It aids in interpreting results from intricate frameworks and uncovering nonlinear relationships between features and model outputs.

References

- [1] Mardani-Aghabaglou, A., Andiç-Çakir, Ö., and Ramyar, K. (2013) Freeze-thaw resistance and transport properties of high-volume fly ash roller compacted concrete designed by maximum density method. *Cement and Concrete Composites*. 37 (1), 259–266.
- [2] Algin, Z. and Gerginci, S. (2020) Freeze-thaw resistance and water permeability properties of roller compacted concrete produced with macro synthetic fibre. *Construction and Building Materials*. 234 117382.
- [3] Vahedifard, F., Nili, M., and Meehan, C.L. (2010) Assessing the effects of supplementary cementitious materials on the performance of low-cement roller compacted concrete pavement. *Construction and Building Materials*. 24 (12), 2528–2535.
- [4] Moradi, S. and Shahnoori, S. (2021) Eco-friendly mix for Roller-Compacted Concrete: Effects of Persian-Gulf-Dredged marine sand on durability and resistance parameters of concrete. *Construction and Building Materials*. 281 122555.
- [5] Jafarifar, N., Pilakoutas, K., and Bennett, T. (2016) The effect of shrinkage cracks on the load bearing capacity of steel-fibre-reinforced roller-compacted-concrete pavements. *Materials and Structures/Materiaux et Constructions*. 49 (6), 2329–2347.
- [6] Chhorn, C., Hong, S.J., and Lee, S.W. (2017) A study on performance of roller-compacted concrete for pavement. *Construction and Building Materials*. 153 535–543.
- [7] Aghaeipour, A. and Madhkhan, M. (2020) Mechanical properties and durability of roller compacted concrete pavement (RCCP)—a review. *Road Materials and Pavement Design*. 21 (7), 1775–1798.
- [8] Zhu, X., Bai, Y., Chen, X., Tian, Z., and Ning, Y. (2022) Evaluation and prediction on abrasion resistance of hydraulic concrete after exposure to different freeze-thaw cycles. *Construction and Building Materials*. 316 126055.
- [9] Hazaree, C., Ceylan, H., and Wang, K. (2011) Influences of mixture composition on properties and freeze-thaw resistance of RCC. *Construction and Building Materials*. 25 (1), 313–319.
- [10] Delatte, N. and Storey, C. (2005) Effects of Density and Mixture Proportions on Freeze–Thaw Durability of Roller-Compacted Concrete Pavement. *Transportation Research Record: Journal of the Transportation Research Board*. 1914 (1), 45–52.
- [11] Rahmani, E., Sharbatdar, M.K., and H.A.Beygi, M. (2020) A comprehensive investigation into the effect of water to cement ratios and cement contents on the physical and mechanical properties of Roller Compacted Concrete Pavement (RCCP). *Construction and Building Materials*. 253 119177.
- [12] Fakhri, M. and Amoosoltani, E. (2017) The effect of Reclaimed Asphalt Pavement and crumb rubber on mechanical properties of Roller Compacted Concrete Pavement.

- Construction and Building Materials. 137 470–484.
- [13] Yildizel, S.A., Calis, G., and Tayeh, B.A. (2020) Mechanical and durability properties of ground calcium carbonate-added roller-compacted concrete for pavement. *Journal of Materials Research and Technology*. 9 (6), 13341–13351.
- [14] Hani, N., Nawawy, O., Ragab, K.S., and Kohail, M. (2018) The effect of different water/binder ratio and nano-silica dosage on the fresh and hardened properties of self-compacting concrete. *Construction and Building Materials*. 165 504–513.
- [15] Fallah, S. and Nematzadeh, M. (2017) Mechanical properties and durability of high-strength concrete containing macro-polymeric and polypropylene fibers with nano-silica and silica fume. *Construction and Building Materials*. 132 170–187.
- [16] ACI (American Concrete Institute) (1995) State of the-art report on roller compacted concrete pavement. in: .
- [17] Hashemi, M., Shafigh, P., Asadi, I., Mahpour, A., and Samadian, A. (2022) The effect of superplasticizer admixture on the engineering characteristics of roller-compacted concrete pavement. *International Journal of Pavement Engineering*. 23 (7), 2432–2447.
- [18] 12390-3, U.N.I.E.N. (2003) Testing Hardened Concrete □ Compressive Strength of Test Specimens. in: .
- [19] C496, A. (2004) Standard Test Method For Splitting Tensile Strength of Cylindrical Concrete Specimens.
- [20] C666, A. (2004) Standard test method for resistance of concrete to rapid freezing and thawing.
- [21] C597, A. (2004) Standard test method for pulse velocity through concrete.
- [22] C642, A. (2013) Standard Test Method for Density, Absorption, and Voids in Hardened Concrete.
- [23] Quercia, G., Hüsken, G., and Brouwers, H.J.H. (2012) Water demand of amorphous nano silica and its impact on the workability of cement paste. *Cement and Concrete Research*. 42 (2), 344–357.
- [24] Fernández, J.M., Duran, A., Navarro-Blasco, I., Lanas, J., Sirera, R., and Alvarez, J.I. (2013) Influence of nanosilica and a polycarboxylate ether superplasticizer on the performance of lime mortars. *Cement and Concrete Research*. 43 (1), 12–24.
- [25] Senff, L., Hotza, D., Repette, W.L., Ferreira, V.M., and Labrincha, J.A. (2010) Mortars with nano-SiO2 and micro-SiO2 investigated by experimental design. *Construction and Building Materials*. 24 (8), 1432–1437.
- [26] Zhang, M.H., Islam, J., and Peethamparan, S. (2012) Use of nano-silica to increase early strength and reduce setting time of concretes with high volumes of slag. *Cement and Concrete Composites*. 34 (5), 650–662.
- [27] Du, H., Du, S., and Liu, X. (2014) Durability performances of concrete with nano-silica. *Construction and Building Materials*. 73 705–712.

- [28] Ghafari, E., Costa, H., Júlio, E., Portugal, A., and Durães, L. (2014) The effect of nanosilica addition on flowability, strength and transport properties of ultra high performance concrete. *Materials and Design*. 59 1–9.
- [29] Kumar, S., Kumar, A., and Kujur, J. (2019) Influence of nanosilica on mechanical and durability properties of concrete. *Proceedings of the Institution of Civil Engineers Structures and Buildings*. 172 (11), 781–788.
- [30] Abhilash, P.P., Nayak, D.K., Sangoju, B., Kumar, R., and Kumar, V. (2021) Effect of nano-silica in concrete; a review. *Construction and Building Materials*. 278 122347.
- [31] Nili, M. and Ehsani, A. (2015) Investigating the effect of the cement paste and transition zone on strength development of concrete containing nanosilica and silica fume. *Materials and Design*. 75 174–183.
- [32] Tavakoli, D., Sakenian Dehkordi, R., Divandari, H., and de Brito, J. (2020) Properties of roller-compacted concrete pavement containing waste aggregates and nano SiO2. *Construction and Building Materials*. 249 118747.
- [33] Chhorn, C., Hong, S.J., and Lee, S.W. (2018) Relationship between compressive and tensile strengths of roller-compacted concrete. *Journal of Traffic and Transportation Engineering (English Edition)*. 5 (3), 215–223.
- [34] Abd Elrahman, M., Chung, S.-Y., Sikora, P., Rucinska, T., and Stephan, D. (2019) Influence of Nanosilica on Mechanical Properties, Sorptivity, and Microstructure of Lightweight Concrete. *Materials*. 12 (19), 3078.
- [35] Younis, K.H. and Mustafa, S.M. (2018) Feasibility of Using Nanoparticles of SiO2 to Improve the Performance of Recycled Aggregate Concrete. *Advances in Materials Science and Engineering*. 2018.
- [36] Isfahani, F.T., Redaelli, E., Lollini, F., Li, W., and Bertolini, L. (2016) Effects of Nanosilica on Compressive Strength and Durability Properties of Concrete with Different Water to Binder Ratios. *Advances in Materials Science and Engineering*. 2016.
- [37] Said, A.M., Zeidan, M.S., Bassuoni, M.T., and Tian, Y. (2012) Properties of concrete incorporating nano-silica. *Construction and Building Materials*. 36 838–844.
- [38] Mohammed, B.S., Awang, A.B., Wong, S.S., and Nhavene, C.P. (2016) Properties of nano silica modified rubbercrete. *Journal of Cleaner Production*. 119 66–75.
- [39] Elemam, W.E., Abdelraheem, A.H., Mahdy, M.G., and Tahwia, A.M. (2020) Optimizing fresh properties and compressive strength of self-consolidating concrete. *Construction and Building Materials*. 249 118781.
- [40] Ting, M.Z.Y., Wong, K.S., Rahman, M.E., and Selowarajoo, M. (2021) Prediction model for hardened state properties of silica fume and fly ash based seawater concrete incorporating silicomanganese slag. *Journal of Building Engineering*. 41 102356.
- [41] Awolusi, T.F., Oke, O.L., Akinkurolere, O.O., and Sojobi, A.O. (2019) Application of

- response surface methodology: Predicting and optimizing the properties of concrete containing steel fibre extracted from waste tires with limestone powder as filler. *Case Studies in Construction Materials*. 10 e00212.
- [42] Elsheikh, A.H., Sharshir, S.W., Abd Elaziz, M., Kabeel, A.E., Guilan, W., and Haiou, Z. (2019) Modeling of solar energy systems using artificial neural network: A comprehensive review. *Solar Energy*. 180 622–639.
- [43] Meng, E., Huang, S., Huang, Q., Fang, W., Wu, L., and Wang, L. (2019) A robust method for non-stationary streamflow prediction based on improved EMD-SVM model. *Journal of Hydrology*. 568 462–478.
- [44] Nematzadeh, M., Shahmansouri, A.A., and Zabihi, R. (2021) Innovative models for predicting post-fire bond behavior of steel rebar embedded in steel fiber reinforced rubberized concrete using soft computing methods. *Structures*. 31 1141–1162.
- [45] Lee, S., Lee, K.K., and Yoon, H. (2019) Using artificial neural network models for groundwater level forecasting and assessment of the relative impacts of influencing factors. *Hydrogeology Journal*. 27 (2), 567–579.
- [46] Guijo-Rubio, D., Durán-Rosal, A.M., Gutiérrez, P.A., Gómez-Orellana, A.M., Casanova-Mateo, C., Sanz-Justo, J., et al. (2020) Evolutionary artificial neural networks for accurate solar radiation prediction. *Energy*. 210 118374.
- [47] Ghorbani, B., Arulrajah, A., Narsilio, G., Horpibulsuk, S., and Bo, M.W. (2020) Development of genetic-based models for predicting the resilient modulus of cohesive pavement subgrade soils. *Soils and Foundations*. 60 (2), 398–412.
- [48] Shahin, M.A., Maier, H.R., and Jaksa, M.B. (2004) Data Division for Developing Neural Networks Applied to Geotechnical Engineering. *Journal of Computing in Civil Engineering*. 18 (2), 105–114.
- [49] Ghorbani, B., Arulrajah, A., Narsilio, G., and Horpibulsuk, S. (2020) Experimental investigation and modelling the deformation properties of demolition wastes subjected to freeze–thaw cycles using ANN and SVR. *Construction and Building Materials*. 258 119688.
- [50] Lundberg, S.M., Allen, P.G., and Lee, S.-I. (2017) A Unified Approach to Interpreting Model Predictions. .
- [51] Nordin, N., Zainol, Z., Mohd Noor, M.H., and Chan, L.F. (2023) An explainable predictive model for suicide attempt risk using an ensemble learning and Shapley Additive Explanations (SHAP) approach. *Asian Journal of Psychiatry*. 79 103316.